Tumor detection and elimination by a targeted gallium corrole

Hasmik Agadjanian[a], Jun Ma[a], Altan Rentsendorj[a], Vinod Valluripalli[a], Jae Youn Hwang[b], Atif Mahammed[c], Daniel L. Farkas[b,1], Harry B. Gray[d,1], Zeev Gross[c,1], and Lali K. Medina-Kauwe[a,e,1]

[a]Department of Biomedical Sciences and [b]Minimally Invasive Surgical Technologies Institute and Department of Surgery, Cedars-Sinai Medical Center, Los Angeles, CA 90048; [d]Beckman Institute, California Institute of Technology, Pasadena, CA 91125; [c]Schulich Faculty of Chemistry, Technion-Israel Institute of Technology, Haifa 32000, Israel; and [e]Geffen School of Medicine, University of California, Los Angeles, CA 90095

Contributed by Harry B. Gray, February 15, 2009 (sent for review December 18, 2008)

Sulfonated gallium(III) corroles are intensely fluorescent macrocyclic compounds that spontaneously assemble with carrier proteins to undergo cell entry. We report in vivo imaging and therapeutic efficacy of a tumor-targeted corrole noncovalently assembled with a heregulin-modified protein directed at the human epidermal growth factor receptor (HER). Systemic delivery of this protein-corrole complex results in tumor accumulation, which can be visualized in vivo owing to intensely red corrole fluorescence. Targeted delivery in vivo leads to tumor cell death while normal tissue is spared. These findings contrast with the effects of doxorubicin, which can elicit cardiac damage during therapy and required direct intratumoral injection to yield similar levels of tumor shrinkage compared with the systemically delivered corrole. The targeted complex ablated tumors at >5 times a lower dose than untargeted systemic doxorubicin, and the corrole did not damage heart tissue. Complexes remained intact in serum and the carrier protein elicited no detectable immunogenicity. The sulfonated gallium(III) corrole functions both for tumor detection and intervention with safety and targeting advantages over standard chemotherapeutic agents.

heregulin | human epidermal growth factor receptor | cancer | in vivo imaging | porphyrinoids

Cancer is on track to overtake heart disease as the number 1 cause of death worldwide next year. Chemotherapy has been increasingly successful in treating this disease, but progress has been slower than desired. Collaborative efforts of all relevant disciplines will be required to enhance treatment efficacy and facilitate quantitative dynamic monitoring (1). A case in point is our potentially powerful technology combining both detection and treatment in a single self-assembled complex between a targeted cell penetration protein and a sulfonated gallium(III) corrole. The intensely red corrole fluorescence enables complex tracking in vivo.

The 2,17-bis-sulfonated corrole and its metal complexes share similarities with porphyrins and related macrocycles that are currently being explored for cancer therapy (2, 3), but their recently revealed properties suggest distinct advantages over other compounds. Specifically, these corroles are water soluble (thus enabling facile use in physiological fluids), do not require photoexcitation to elicit cytotoxicity (thus expanding the potential tissue depth and distance at which corrole-mediated therapy may be administered), are unable to enter cells without the aid of a carrier molecule (thus aiding the specificity of delivery), and bind to cell-targeting proteins in a very tight, spontaneous and noncovalent fashion (4, 5). Accordingly, we have explored the possibility of assembling targeted corrole complexes with modified cell targeting ligands previously studied for tumor-targeted cell penetration (6, 7). After screening several of our cell targeted proteins against a panel of metallated and nonmetallated corroles (6, 7), we selected the combination of a breast cancer-targeted cell penetration protein (HerPBK10) and a sulfonated gallium-metallated corrole (S2Ga), based on the unique features of each component. S2Ga forms a tight assembly with the carrier protein that resists high-speed centrifugation and transfer to albumin, brightly fluoresces, and induces toxicity to target cells after delivery and uptake by the carrier (6). Importantly, corrole cytotoxicity is best supported by a membrane penetrating function, because nonpenetrating carriers such as albumin did not enable sufficient cytotoxicity (6). This suggests that sulfonated corroles entering cells via receptor-mediated endocytosis must somehow escape the endosomal vesicle to induce cytotoxicity (6). The protein used in these studies provides both the targeting and penetration required for effective corrole delivery.

HerPBK10 contains the receptor-binding domain of heregulin-αB_{1B} fused amino (N) terminally to a modified adenovirus (Ad) penton base capsid protein (7). The heregulin-derived moiety has been used to direct nonviral and viral gene delivery to $HER2^+$ cells in vitro (7, 8). The same ligand segment produced as a recombinant fusion to green fluorescent protein (GFP) shows preferential accumulation in $HER2^+$ tumors in mice when delivered intravenously (Fig. S1). This ligand also induces rapid endocytosis after receptor binding, thus enabling entry of attached molecules into the target cell (9, 10). As vesicle-entrapped ligands typically become degraded by lysosomal enzymes or recycle back to the cell surface (which would both reduce efficacy if used to deliver a therapeutic payload), the penton base moiety of HerPBK10 contributes an endosomolytic function to facilitate release of internalized particles into the cytoplasm after uptake, thus enhancing therapeutic efficacy.

One important feature of HerPBK10 is that it binds and enters $HER2^+$, but not $HER2^-$, human breast cancer cells in vitro (6, 7) (Fig. S2). $HER2^+$ breast tumors are characterized by an amplification of the HER2 subunit and predict a poor prognosis, resistance to chemotherapy, tumor recurrence, and high mortality (11, 12). Normal mammary cells express low levels of HER2 localized mainly in the cytoplasm, whereas HER2 amplification yields high levels displayed on the cell surface, and enhanced mitogenic signaling, thus making the receptor a high-profile landing pad for targeting. Monoclonal antibodies directed against the extracellular domain of HER2 can influence cancer growth, but have limitations in their ability to modulate HER2 signaling (13, 14). Moreover, these antibodies can bind tissues with normal HER2 levels, such as the myocardium, and thus interfere with signaling for normal tissue maintenance. When used in combination with conventional chemotherapeutic

Author contributions: H.A., D.L.F., H.B.G, Z.G., and L.K.M.-K. designed research; H.A., J.M., A.R., V.V., J.Y.H., and A.M. performed research; A.M., D.L.F., H.B.G., Z.G., and L.K.M.-K. contributed new reagents/analytic tools; H.A., D.L.F., Z.G., and L.K.M.-K. analyzed data; and D.L.F., H.B.G., Z.G., and L.K.M.-K. wrote the paper.

The authors declare no conflict of interest.

[1]To whom correspondence may be addressed. E-mail: hbgray@caltech.edu, daniel.farkas@cshs.org, chr10zg@tx.technion.ac.il, or lali.medinakauwe@cshs.org.

This article contains supporting information online at www.pnas.org/cgi/content/full/0901531106/DCSupplemental.

agents, such as doxorubicin, the adverse myocardial effects are exacerbated, because doxorubicin alone also induces cardiac damage (15–17). Although heregulin interacts directly with HER3 or HER4 subunits, but not HER2 (18), ligand affinity is greatly enhanced by HER2, which should enable therapies targeted at the receptor heterodimer. Accordingly, such ligand-directed therapies are likely to accumulate at HER2-amplified heterodimers and avoid tissues displaying normal HER2 levels.

Here, we take advantage of HER ligand-receptor interaction and endocytosis to deliver therapeutics into the cell and elicit cell death from within, rather than trying to modulate signaling from the cell surface. We rely on our previous findings showing that noncovalent assemblies formed between HerPBK10 and sulfonated corroles resist serum-induced destabilization and induce targeted cell death in culture (6). We have focused our efforts on developing targeted assemblies using S2Ga for 2 reasons: this corrole was found to be the most toxic derivative (6) and its intense fluorescence suggested that it could be very useful for imaging purposes. Here, we report that a HER-targeted noncovalent corrole assembly formed between HerPBK10 and S2Ga (HerPBK10-S2Ga or HerGa) accumulates in HER2$^+$ cells and induces tumor-targeted toxicity in a mixed cell population in vitro as well as in vivo. Notably, we demonstrate the tumor-targeting effect of HerPBK10 by whole animal imaging, and report highly effective tumor-growth regression in mice with no detectable effect on off-target tissues such as the heart and no carrier protein immunogenicity.

Results

Corrole Fluorescence Enables Tracking of Tumor Targeting and Intracellular Distribution. The ability to detect corrole fluorescence in vivo allows not only the potential to detect tumors but also tracks tumor targeted therapy in a live specimen. Here, we assess HerGa targeting capacity in female nude mice bearing human HER2$^+$ tumors on each flank. Mice received a single tail vein injection of either HerGa or S2Ga alone, and the mice were imaged in real time using a custom fluorescence bioimager (19). Whereas S2Ga fluorescence exhibited a broad systemic distribution throughout most of the mouse and appeared to be excluded from the tumors, HerGa showed a preferential accumulation in the tumors and a much lower distribution to extratumoral areas compared with free S2Ga (Fig. 1*A*). A high fluorescence signal in the tail region of both mice resulted from some material inadvertently becoming deposited in the tail muscle flanking the site of injection. Images acquired at sequential time points in real time after tail vein injection show that HerGa accumulates rapidly at tumor sites within minutes after administration (Fig. 1*B*). Corrole fluorescence detected at the cellular level enables intracellular tracking of the complex in target cells. Here, we can observe punctate corrole fluorescence (Fig. 1*C*) transition over time to diffuse fluorescence (Fig. 1*D*) during HerGa entry into live HER2$^+$ MDA-MB-435 human cancer cells (suggestive of endocytic uptake followed by vesicle leakage into the perinuclear cytosol), and cytosolic retention/nuclear exclusion is visible up to at least 24 hr after HerGa uptake in the same cells (Fig. 1*E*).

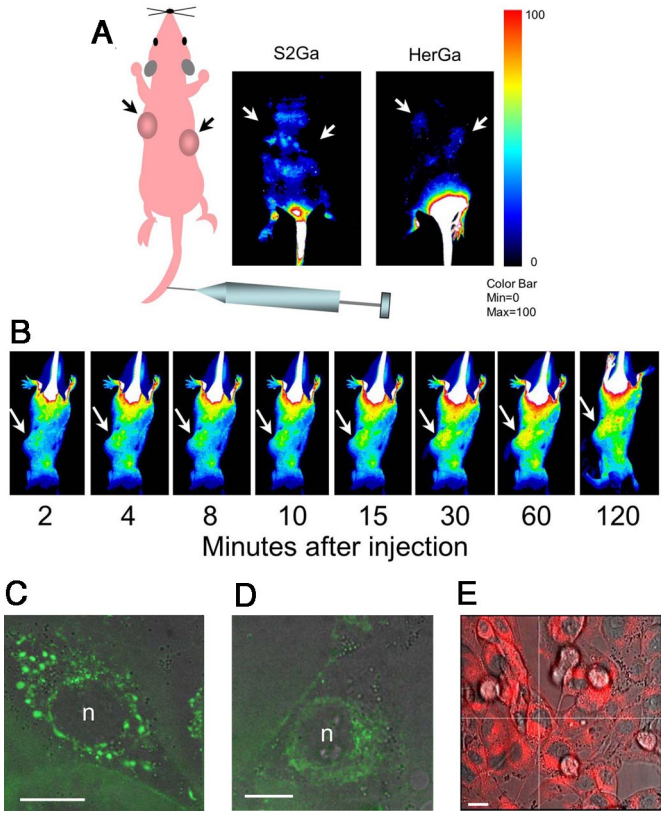

Fig. 1. Detection of HerGa in vivo targeting and intracellular trafficking. Live animal imaging of corrole fluorescence after IV delivery of either free corrole or targeted complex. (*A*) Nude mice bearing human HER2$^+$ tumors (≈300 cubic mm) received a single IV injection of either S2Ga or HerGa (15 nmoles with respect to corrole dose) and were imaged at 2.5 hr postinjection using a noninvasive small animal fluorescence imaging system (35). Schematic to the left indicates the whole body and tumor orientation of the mice in the fluorescent images. (*B*) Images capturing time course of corrole circulation in mice after receiving HerGa as described in *A*. Arrows in both *A* and *B* point to tumors. Corrole fluorescence is indicated by blue-red pseudocoloring with fluorescence intensity represented according to the color bar on the right. (*C–E*) Intracellular trafficking in live cells. MDA-MB-435 cells were treated with HerGa at 1 μM final corrole concentration and live cells imaged by fluorescence microscopy at the indicated time points after treatment. (*C* and *D*) High-resolution spinning disk micrographs (Perkin-Elmer/Improvision) showing apparent vesicles and corrole fluorescence (pseudocolored green) distribution in cytoplasm at 15 min (*C*) and 2 hr (*D*). (*E*) Micrograph of corrole fluorescence (red) distribution in cytoplasm as captured by inverted fluorescence microscopy at up to 24 hr after uptake. In *C–E*, fluorescence images were overlaid on brightfield images. n, nucleus. (Scale bars, 10 μm.)

Targeted Corrole Ablates Tumor Cells in Vitro and in Vivo. We have previously shown that HerGa specifically bound and entered HER2$^+$ MDA-MB-435 but not HER2$^-$ MDA-MB-231 human cancer cells in separate cell cultures, and induced HER2$^+$ but not HER2$^-$ cell death (6). Here, we introduce a further challenge by testing the ability of HerGa to target HER2$^+$ cells in a mixed culture of HER2$^+$ and HER2$^-$ cells. To identify each cell line in coculture, the HER2$^-$ cells were tagged with a GFP marker (Fig. 2 *Top*). We treated these mixed cultures daily with either HerGa or with the equivalent concentration of S2Ga alone (0.5 μM) and measured cell survival each day. Whereas HerGa reduced HER2$^+$ but not HER2$^-$ cell counts (Fig. 2*B*), S2Ga had little effect on either cell line (Fig. 2*C*). The cytotoxic positive control, doxorubicin, was not as discriminatory between the 2 cell lines, and in fact, was less effective on the HER2$^+$ cells (Fig. 2*D*). HerPBK10 alone had no cytotoxic effect (Fig. 2*A*), indicating that HerPBK10 contributes to targeting and is required for S2Ga to elicit toxicity.

Ideally, targeting should afford the ability to administer a therapeutic systemically and induce toxicity to tumor cells while sparing normal tissue. To test this, we examined the therapeutic efficacy of HerGa by measuring tumor volumes up to 25 days after mice received daily tail vein injections of HerGa or controls for 7 days. Tail vein injections were initiated once tumors reached a size of ≈250–300 cubic mm (≈3–4 weeks after s.c. tumor inoculation) (Fig. 3*A*). Whereas tumor growth was unaffected in mice receiving saline or HerPBK10 alone, S2Ga appeared to have a modest reducing effect on tumor growth.

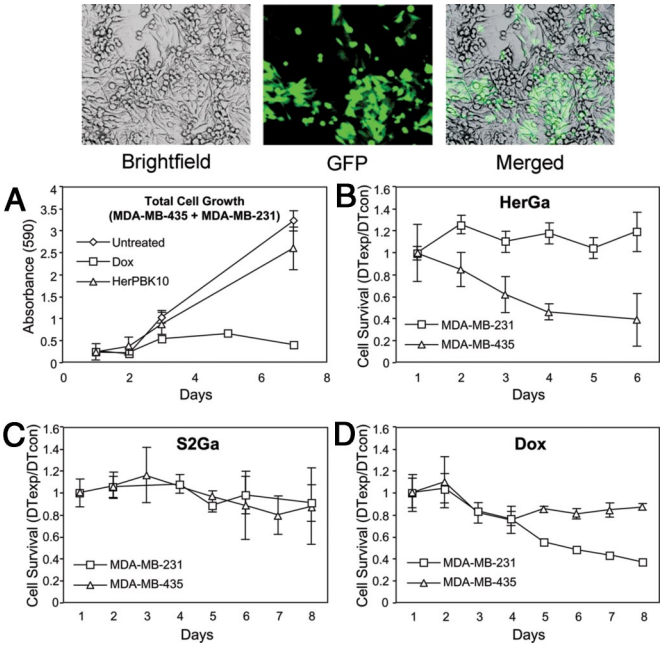

Fig. 2. Targeted cytotoxicity in a mixed culture of HER2$^+$ and HER2$^-$ human cancer cells. Cell cultures containing 1:1 cell ratio of MDA-MB-435 (ErbB2$^+$,GFP$^-$):MDA-MB-231 (ErbB2$^-$,GFP$^+$) (*Top*) were treated with HerPBK10 alone (*A*), HerPBK10-S2Ga (*B*), S2Ga (*C*), or doxorubicin (Dox) (*D*) at 0.5 μM final drug (corrole or Dox) concentration. HerPBK10 alone was added at the equivalent concentration to the same protein in the complex. Cells were treated daily for 1 week in complete (serum-containing) medium and cells assessed at the indicated time points for GFP fluorescence (to determine relative MDA-MB-231 number) and crystal violet staining (to determine total cell number). Cell survival was determined by calculating the relative doubling time (DT) of experimental (exp) cells normalized by control (con) cells based on the crystal violet stains (total cells) and GFP fluorescence (MDA-MB-231 cells). The DT of MDA-MB-435 was determined by subtracting the DT of MDA-MB-231 from the total cell DT.

However, HerGa not only prevented tumor growth but appeared to reduce the size of the tumors that were already established at the time of treatment (Fig. 3*B*). Importantly, i.v. HerGa treatment showed greater therapeutic efficacy at 5 times the lower dose compared with free doxorubicin delivered systemically, because 0.04 mg/kg Dox merely reduced tumor growth (Fig. 3*C*) whereas 0.008 mg/kg HerGa not only inhibited tumor growth but also elicited some shrinkage. Significant tumor shrinkage by doxorubicin could only be observed if mice received relatively high doses (2.5 mg/kg) injected intratumorally (Fig. 3*C*), thus implying that systemic HerGa has similar effect to nearly 300 times higher doses of doxorubicin delivered intratumorally.

To examine whether off-target tissues such as the heart were affected, mice were euthanized on the last day of tumor measurement and tissues were harvested for histological examination. We compared hearts of treated mice to that of mice receiving intratumoral injections of doxorubicin, which is known to induce cardiotoxicity. Despite its local delivery, doxorubicin-treated mice exhibited typical cardiomyopathy, including focal degeneration and myofibrillar loss as observed elsewhere (20, 21), whereas mice receiving S2Ga or HerGa showed no signs of myocardial damage, similar to saline-treated mice (Fig. 3*D*). HerPBK10 alone also had no effect on myocardium histology.

Preimmune and Postimmune Serum Do Not Affect Targeting or Stability. To address concerns regarding the use of an adenovirus capsid protein-derived carrier for the corrole, we examined whether HerPBK10 induced the formation of neutralizing antibodies. A single inoculation of Ad can produce a long-lasting humoral response in patients (22) and animals (23), and prevent subsequent administration, thus reducing overall therapeutic efficacy. Here, we tested the antibody formation potential of HerPBK10 under the same conditions that produce an Ad capsid-elicited humoral response (24). Immune competent (C57BL/6) mice were inoculated with HerPBK10 at an equiva-

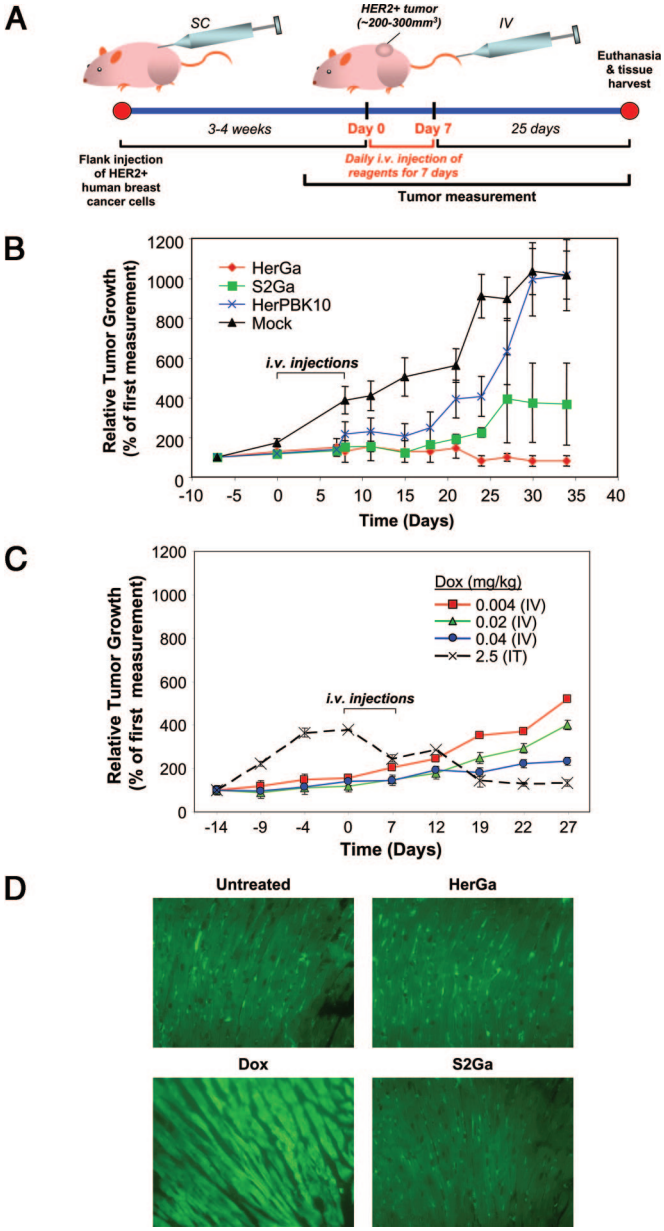

Fig. 3. Targeted tumor growth intervention by HerGa. Effect of systemically-delivered HerGa or individual components on tumor growth. Nude mice bearing HER2$^+$ tumors received daily IV injections for 1 week of the indicated reagents when the tumors reached 250–300 cubic mm (tumor inoculation and treatment schedule depicted in *A*; SC, subcutaneous). Graph in *B* presents tumor volumes measured before, during, and after treatment. Mice were euthanized at 25 days after the last day of treatment, and tissues harvested for histological assessment. $n = 5$–9 tumors per treatment group. (*C*) Comparative doses of Dox delivered IV or intratumorally (IT) on tumor growth. Treatment schedule is the same as in *B*. (*D*) Effect on myocardia of hearts harvested from treated mice at the end of the experiments in *B* and *C* (''Dox'' hearts were harvested from mice receiving Dox IT). Paraffin-fixed specimens were processed for immunofluorescence against myosin and imaged at 60× magnification.

lent HerGa therapeutic dose (0.05 mg/kg with regard to protein dose) as well as a 10-fold higher dose (0.5 mg/kg). As a comparison, mice were also inoculated with Ad5 at a dose established elsewhere (24) to induce neutralizing antibody formation (1.2×10^9 pfu per mouse). Blood was collected from mice before the initial antigen inoculation, followed by blood collections every 7 days up to 35 days after the initial inoculation, whereas mice received a second inoculation of the same antigens on day 21 to boost any existing immunity (Fig. 4*A Upper*, timeline). Both doses of HerPBK10 produced no significant induction of anti-HerPBK10 antibodies compared with untreated mice, whereas the dose of Ad5 triggered secretion of antibodies that recognize HerPBK10 (Fig. 4*A Lower*). To assess whether these antibodies actually prevent HerPBK10 binding to target cells, receptor-ligand binding was measured by attachment capacity of MDA-MB-435 cells to HerPBK10-coated plates in immune serum. Compared with cells attached in complete media, preimmune serum did not prevent, and even modestly enhanced, cell attachment ($P = 0.03$), and the level of attachment in sera from either Ad5- or HerPBK10-treated mice was comparable to that in preimmune serum (Fig. 4*B*). The apparent increase in binding is unexpected and may be due to composition differences between mouse serum and complete media containing bovine serum. The ability of recombinant heregulin ligand, Her, to inhibit cell attachment ($P < 0.01$ compared with binding in preimmune serum, as determined by a 2-tailed unpaired *t* test), verified that attachment takes place via heregulin receptors (Fig. 4*B*). Overall, these findings indicate that whereas Ad5 can generate antibodies against HerPBK10, this is not enough to prevent binding of HerPBK10 to target cells.

Another in vivo concern regards the potential for premature corrole release from the complex and its transfer to serum in blood. Our previous studies have shown that corrole complexes do not transfer the corrole to immobilized serum albumin in vitro (6). To predict HerGa stability in vivo, we incubated the complex up to 1 hr at 37 °C on immobilized human serum, then removed the complex from the immobilized substrate and assessed how much corrole is lost from the complex by comparing the fluorescence after incubation on the immobilized sera with the input fluorescence. We detected negligible loss of corrole fluorescence from HerGa whereas S2Ga alone, which is expected to bind readily to the serum proteins, exhibited considerable loss to the immobilized serum ($P < 0.03$ compared with incubation without serum) (Fig. 4*C*).

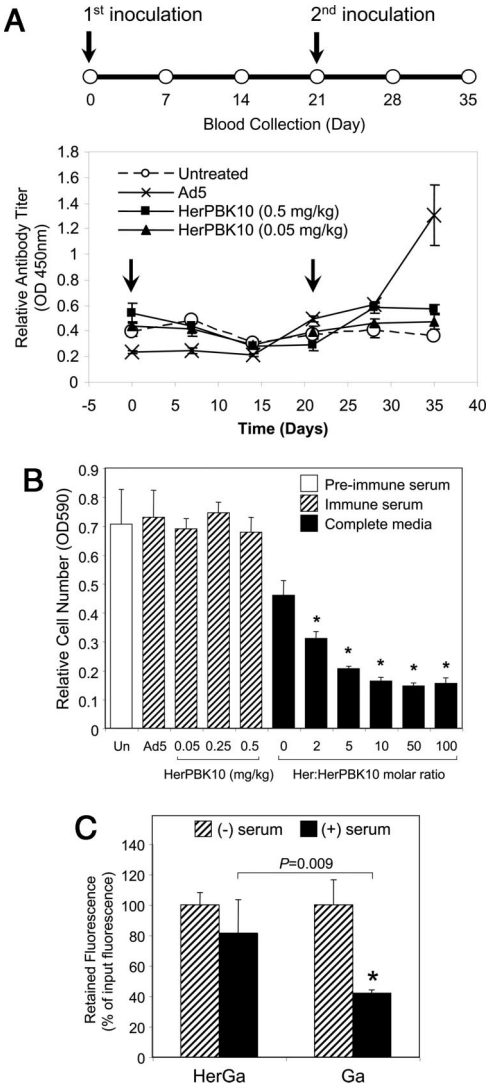

Fig. 4. Neutralizing antibody induction and serum stability. (*A*) Immunocompetent (C57BL/6) mice received an initial s.c. inoculation of HerPBK10 protein (0.05 or 0.5 mg/kg) or Ad5-GFP (1.2×10^9 pfu per mouse) followed by blood collection scheduled every 7 days up to day 35 after the initial inoculation as summarized by the time chart (*Upper*). On day 21, respective mice received a second inoculation of each corresponding reagent. Sera isolated from bleeds were assessed by ELISA for relative antibody titer produced against HerPBK10 (*Lower*). Arrows denote days of antigen inoculation. $n = 4$ mice per treatment group dose. (*B*) Effect of immune sera on target cell binding. Ligand-receptor binding was tested by measuring the level of cell attachment to HerPBK10-coated plates in immune or preimmune serum collected from mice in *A*. Cells suspended in either preimmune serum, immune serum from Ad5 or HerPBK10-inoculated mice, or complete media containing 10% bovine serum but no mouse serum were incubated on HerPBK10-coated wells for 1 hr at 37 °C, followed by removal of free cells and measurement of attached cells by crystal violet assay. The level of receptor-specific binding was assessed on separate cells preincubated with competitive inhibitor (Her). Un, untreated mice. *, $P < 0.01$ compared with cells attached in preimmune serum, as determined by the 2-tailed unpaired *t* test. (*C*) Relative corrole retention by HerGa during incubation in human serum. Human serum (Omega Scientific, Inc.) was immobilized by overnight incubation at 4 °C in 96-well plates. The next day, the wells were washed with PBS, and HerGa or S2Ga alone (50 μM final) were added to each well. After incubation at 37 °C for the indicated time points, samples were removed from the wells and measured for corrole fluorescence. Corrole retention or loss by the complex was assessed by comparing the fluorescence of preserum and postserum incubation samples (RFU 424 nm excitation wavelength/620 nm emission wavelength of postincubation sample/input). Fluorescence values are shown as a percentage of input fluorescence (of fluorescence of complex before serum incubation). *, $P < 0.03$ compared with incubation without serum. Significances were determined by 2-tailed paired *t* tests.

Discussion

Existing approaches to targeting therapeutic agents or drugs require linking the compound to the targeted carrier by 1 or more covalent bonds. Such chemical modifications complicate preparation of the conjugate and entail high costs, and also can compromise the potency of the drug and abrogate the activity or specificity of the carrier molecule. Instead, a system in which the therapeutic agent can be incorporated with a carrier and then may be released into the target cell would be greatly preferred. Earlier we demonstrated that this is possible by combining the targeting and cell penetrating features of the HerPBK10 recombinant protein with corroles that can spontaneously assemble with carrier molecules to form a new type of noncovalent nanoparticle. Our previous in vitro investigations strongly indicated that HER-targeted corrole particles specifically bind, enter, and kill $HER2^+$ but not $HER2^-$ cells in separate cultures (6). Here, we show that $HER2^+$ cells can even be targeted in a mixed culture of $HER2^+$ and $HER2^-$ cells. The ability to track our targeted particle in vivo by fluorescence has allowed us to demonstrate that it localizes in $HER2^+$ tumors in vivo and elicits tumor cell death. Importantly, established tumors undergo not only growth prevention but also a reduction in volume, and these desirable outcomes are achieved while sparing important tissues

such as the heart, which can otherwise undergo adverse effects from similar HER2-targeted treatments (15–17)

We have shown that corroles are superior to porphyrins and related compounds for some applications. For example, Photofrin (a porphyrin derivative) is used as a photosensitizer, requiring light of a specific wavelength to induce damage to tumor cells after intratumoral accumulation (25). In contrast, we have found (6) that corroles do not require photoexcitation to induce cytotoxicity. Porphyrin derivatives have suboptimal absorption for maximal tissue penetration, and are readily oxidized (26), thus drastically limiting their use. Because photoexcitation is not required for cell killing, corroles potentially could be used effectively in a variety of in vivo sites. Whereas Photofrin contains a complex mixture of ether- and ester-linked dimers and higher oligomers, raising drug regulatory concerns, corroles can be used as water-soluble molecules (27) for use under physiological conditions.

Corroles also may have therapeutic and safety advantages over currently used drugs such as doxorubicin and cisplatin, whose mechanisms of action require nuclear entry to bind DNA and inhibit replication (28). These drugs are nondiscriminatory and can permeate nearly any cell, but are most potent to dividing cells (i.e., tumor tissue, but also bone marrow, hair, and gastrointestinal tract epithelia). Nevertheless, damage to nondividing cells is possible, as exemplified by the serious cardiotoxicity and cytoskeletal damage incurred by doxorubicin on heart tissue (29, 30). In contrast, the inability of corroles to penetrate cell membranes without a carrier protein can avoid such detrimental side effects, should the corrole release prematurely from the carrier before reaching a target cell. This is an unlikely possibility, however, due to the high degree of binding stability to endure ultrafiltration, HPLC, and nonexchange with serum protein (5, 6). Our studies here further confirm that the targeted complex retains integrity in human serum, localizes tumors in vivo, and elicits tumor cell death while sparing healthy tissue such as the heart.

Effect on the myocardium has become an important focus regarding the use of HER2-targeted therapeutics in light of the adverse cardiac effects that can be produced by inhibiting HER2 signaling, and that are exacerbated when used in conjunction with doxorubicin (15–17). It is possible that by using the receptor ligand for targeting rather than by using anti-HER2 antibodies prevents homing in on tissues with normal HER2 levels, given that ligand affinity for HER3 or HER4 are enhanced by amplification of HER2 (31–33). In this regard, it may be advantageous to develop targeting agents with intermediate affinities and thus reduce off-target effects while increasing accumulation at tissues displaying amplified levels of the target receptor.

Our approach here is unique in its reliance on noncovalently attached drugs that, through the use of a targeted endosomolytic protein, may be released from endosomal vesicles inside a target cell to induce toxicity. The amphiphilic nature of sulfonated corroles makes this strategy possible by directing the drug to cells targeted by the protein carrier and preventing nonspecific uptake into cells without a protein carrier, thus avoiding detrimental effects to nontargeted cells. Preliminary investigations indicate that traditional apoptosis does not substantially contribute to cell death, whereas cytoskeletal disruption and mitochondrial fragmentation delineate key events of corrole cytotoxicity. A unique feature of the current approach is that the same compound can be used both for imaging and therapeutic intervention, opening new avenues for quantitative in vivo monitoring of chemotherapeutic specificity, topology, dynamics, and effectiveness (34), and thereby paving the way for discovery of even more powerful multifunctional agents for use in the war on cancer.

Materials and Methods

Materials, Cells, and Animals. HerPBK10 protein was produced in and isolated from a bacterial protein expression system as described in ref. 7. Gallium-metallated sulfonated corrole was synthesized, reconstituted in PBS, and quantified as described in ref. 6. MDA-MB-435 and MDA-MB-231 cells were obtained from the National Cancer Institute and maintained at 37 °C in DMEM, 10% FBS at 5% CO_2. Athymic nude and C57BL/6 mice were obtained from Charles River Laboratories, Inc. GFP-tagged cell lines were produced by overnight incubation of cells plated in 6-well dishes with GFP-expressing lentivirus vectors added at 1/3 and 1/9 dilution in 1 mL of complete media with 4 μL of 1 mg/mL protamine sulfate. At 24 hr, cells were washed twice with complete media, and monitored for green fluorescence. Cells were passaged 8 to 9 times to ensure removal of free virus particles before being used for experimental purposes. All mice were euthanized following Institutional Animal Care and Use Committee (IACUC)-approved procedures in accordance with the institutional and national guide for the care and use of laboratory animals.

ELISA. To determine HER2 levels on cell lines, cells plated in 96-well dishes (1×10^4 cells per well) 48 hr earlier were aspirated of medium and briefly washed with PBS, then fixed in 4% PFA/PBS for 12 min at room temperature (RT), followed by washing 3 times with PBS (250 μL per well) before a 1 hr incubation in blocking solution (1% BSA/PBS, 100 μL per well) at RT. Anti-HER2 antibody (rabbit polyclonal anti-erbB-2/Her-2 used at 2 μg/mL; Upstate Biotechnology) was added in triplicate wells (100 μL per well) and incubated for 1 hr at RT, followed by aspiration and washing 3 times with PBS before 1 hr incubation at RT with HRP-conjugated secondary antibody at 1:2,000 dilution. After aspirating secondary antibodies and washing the wells twice with PBS and once with distilled water, the plate was blotted dry and TMB solution was added to each well. The plates were incubated with substrate for ≈30 min (or until the blue color development) in the dark, and the reaction was stopped by adding 100 μL per well 1N HCl. Absorbances were measured at 450 nm in a Spectra Max M2 platereader (Molecular Devices Corp.). To determine mouse serum antibody titer, 96-well plates were coated with HerPBK10 (4 μg per well) in coating buffer (50 mM Na carbonate, pH 9.6) at 4 °C overnight. The next day, wells were washed with 0.05% Tween/PBS and blocked with 5% BSA/PBS for 2 hr at RT. Sera were diluted at 1:10, 1:100, 1:1,000, 1:10,000, and 1:50,000 ratios in 1% BSA/PBS and incubated in separate triplicate wells for 2 hr at RT. After washing to remove free antibody, wells were incubated 2 hr with HRP-conjugated anti-mouse IgG (1:2,000) at RT, then processed for measuring enzyme activity as described earlier.

In Vivo Studies. Female nude mice (6–8 wk) received bilateral flank injections of 1×10^7 MDA-MB-435 human breast cancer cells, after which tumors of ≈250–300 mm^3 were established within 3–4 wk. To obtain real-time imaging of corrole conjugates during systemic delivery, mice received a single i.v. injection of S2Ga or HerPBK10-S2Ga (15 nmol) and were imaged using a real-time in vivo fluorescence image acquisition system developed by D.L.F. (35). A 442 nm laser light was used for the excitation of corrole conjugates, delivered onto the mice through mirrors, enabling uniform excitation of the specimen by scattering the laser light via a 90% transmission broadband diffuser. The emitted light from the mice was imaged by collection using a telecentric lens (MELLES GRIOT, InvaritarTM 59LGL428 and 59LGG950, working distance: 25.7 mm, depth of field: 81.5 mm, NA: 0.24), and passing through standard interference filters (Chroma, 620 nm ± 40 nm) before arriving onto a cooled CCD camera (Princeton Instruments, PIXIS 400) located on top of the light-tight imaging chamber. To test for therapeutic efficacy, mice began receiving daily tail vein injections after tumor establishment for 7 days of S2Ga alone or HerGa (each at 0.008 mg/kg corrole concentration). Control mice received HerPBK10 alone (at the equivalent concentration of protein in HerGa), doxorubicin (at indicated doses and delivery routes), or vehicle (saline) alone. Tumor volumes were measured using calipers for up to 25 days after the final injection, after which mice were euthanized and tissues were harvested for histological assessment [n = 5–9 tumors per treatment; group numbers based on power analysis of similar established studies (36)]. For immune studies, blood from female 6- to 8-week-old C57BL/6 mice was collected before administering a single s.c. injection each of HerPBK10 (0.05 or 0.5 mg/kg) or Ad5 (1.2×10^9 pfu), then mice were bled every 7 days up to 35 days after initial antigen inoculation. The mice received a second inoculation of the same antigens on day 21. Blood was collected in serum separating tubes and centrifuged at 1,000 × g for 10 min to isolate the serum, which was assessed for neutralizing antibody formation by ELISA as described earlier and for receptor binding neutralization by cell attachment, as described in *Cell Attachment Assay*.

Immunohistochemistry of Heart Specimens. Cross-sections (5 μm thickness) of the mid-ventricle areas of paraffin embedded hearts were prepared by AML Labs. Specimens were deparaffinized and rehydrated by washing slides with xylene 3 times 10 min each, followed by a sequential 3 min rinse each in 100%, 90%, 80%, then 70% ethanol. The slides were rinsed 3 times, 2 min each with distilled water, then kept in 0.3% cold methanol for 30 min, followed by washing with PBS 3 times for 2 min. The slides were warmed in 10 mM citrate, pH 6.0 in a 95 °C water bath for 30 min, then cooled for 20 min and rinsed with PBS 3 times for 2 min each. The slides were then blocked in 1% BSA/PBS for 1 hr at RT, followed by incubation with mouse cardiac myosin antibody (Abcam, Inc.) at 1:100 dilution at 4 °C overnight. Next day, the slides were washed 3 times with PBS, followed by incubation with FITC-conjugated anti-mouse antibody (Chemicon International, Inc.) at 1:300 dilution for 1 hr at RT. The slides were washed 3 times with PBS and rinsed in water, then mounted with ProLong Antifade kit (Molecular Probes, Invitrogen).

Cell Attachment Assay. To assess the effect of immune sera on HerPBK10 binding to target cells, separate wells in 96-well plates were coated with HerPBK10 at 4 μg per well by overnight incubation at 4 °C, followed by PBS wash to remove free protein and blocking with 5% BSA/PBS for 2 hr at RT. Meanwhile, MDA-MB-435 cells detached from dishes by 2 mM EDTA/PBS followed by PBS wash were suspended in either complete media (containing 10% bovine serum), sera from immunocompetent mice previously inoculated with antigens as described in Fig. 4*A* (collected on day 35), or preimmune sera from the same mice, and added to separate triplicate wells (at 2×10^4 cells per well) of the HerPBK10-coated plates. To verify the relative level of cell attachment through HER, separate cells were preincubated with recombinant heregulin ligand, or Her, at the indicated molar ratios of Her:HerPBK10 in medium without mouse serum for 30 min with agitation, then plated on HerPBK10-coated plates. The cells were allowed to attach at 37 °C in CO_2 incubators for 1 hr, followed by aspiration of unattached cells, PBS wash, and crystal violet assay to evaluate the relative number of attached cells. For the crystal violet assay, the PBS was aspirated from the wells and replaced with 0.1% crystal violet in 10% ethanol per well. The plate was stained for 15 min at RT, then the stain aspirated and wells washed thoroughly 4 times with 0.2 mL of PBS. The crystal violet was extracted from the cells with 95% ethanol. The optical density (OD) of the samples were detected at 590 nm using a SpectraMax M2 plate reader (Molecular Devices).

ACKNOWLEDGMENTS. We thank Krishnan Ramanujan for helpful feedback and critical review of this work; Kolja Wawrowsky (Cedars-Sinai Medical Center Confocal Core Facility) and Sarah Hamm-Alvarez and Jiansong Xie (University of Southern California Department of Pharmaceutical Sciences) for assistance with microscopic imaging; and Renata Stripecke and Emmanuelle Faure-Kumar (UCLA Vector Core) for provision of adenovirus and lentivirus vectors. This work was supported by National Institutes of Health (NIH) Grants R21 CA116014 and R01 CA102126, Department of Defense Grant BC050662, Susan G. Komen Breast Cancer Foundation Grant BCTR0201194, and a Donna and Jesse Garber Award (all to L.K.M.-K.), and by the U.S. Navy Bureau of Medicine and Surgery (D.L.F.). Work performed at the Technion-Israel Institute of Technology was supported by grants from the Gurwin and Binational Science foundations (to Z.G.). Research at California Institute of Technology was supported by grants from NIH and the National Science Foundation (to H.B.G.).

1. Kawasaki ES, Player A (2005) Nanotechnology, nanomedicine, and the development of new, effective therapies for cancer. *Nanomedicine* 1:101–109.
2. Wang Z, et al. (2007) Synthesis and biologic properties of hydrophilic sapphyrins, a new class of tumor-selective inhibitors of gene expression. *Mol Cancer* 6:9.
3. Chowdhary RK, et al. (2003) Correlation of photosensitizer delivery to lipoproteins and efficacy in tumor and arthritis mouse models; comparison of lipid-based and Pluronic P123 formulations. *J Pharm Sci* 6:198–204.
4. Haber A, et al. (2008) Amphiphilic/bipolar metallocorroles that catalyze the decomposition of reactive oxygen and nitrogen species, rescue lipoproteins from oxidative damage, and attenuate atherosclerosis in mice. *Angew Chem Int Ed Engl* 16:16.
5. Mahammed A, Gray HB, Weaver JJ, Sorasaenee K, Gross Z (2004) Amphiphilic corroles bind tightly to human serum albumin. *Bioconjugate Chem* 15:738–746.
6. Agadjanian H, et al. (2006) Specific delivery of corroles to cells via noncovalent conjugates with viral proteins. *Pharm Res* 23:367–377.
7. Medina-Kauwe LK, Maguire M, Kasahara N, Kedes L (2001) Non-viral gene delivery to human breast cancer cells by targeted Ad5 penton proteins. *Gene Ther* 8:1753–1761.
8. Han X, Kasahara N, Kan YW (1995) Ligand-directed retroviral targeting of human breast cancer cells. *Proc Natl Acad Sci USA* 92:9747–9751.
9. Medina-Kauwe LK, Leung V, Wu L, Kedes L (2000) Assessing the binding and endocytosis activity of cellular receptors using GFP-ligand fusions. *BioTechniques* 29:602–609.
10. Medina-Kauwe LK, Chen X (2002) Using GFP-ligand fusions to measure receptor-mediated endocytosis in living cells. *Vitamins and Hormones*, ed Litwack G (Elsevier Science, San Diego), Vol 65, pp 81–95.
11. Slamon DJ, et al. (1987) Human breast cancer: Correlation of relapse and survival with amplification of the HER-2/neu oncogene. *Science* 235:177–182.
12. Slamon DJ, Clark GM (1988) Amplification of c-erbB-2 and aggressive human breast tumors? *Science* 240:1795–1798.
13. Brodowicz T, et al. (1997) Soluble HER-2/neu neutralizes biologic effects of anti-HER-2/neu antibody on breast cancer cells in vitro. *Int J Cancer* 73:875–879.
14. Xu FJ, et al. (1997) Heregulin and agonistic anti-p185(c-erbB2) antibodies inhibit proliferation but increase invasiveness of breast cancer cells that overexpress p185(c-erbB2): Increased invasiveness may contribute to poor prognosis. *Clin Cancer Res* 3:1629–1634.
15. Keefe DL (2002) Trastuzumab-associated cardiotoxicity. *Cancer* 95:1592–1600.
16. Slamon D, Pegram M (2001) Rationale for trastuzumab (Herceptin) in adjuvant breast cancer trials. *Semin Oncol* 28:13–19.
17. Slamon DJ, et al. (2001) Use of chemotherapy plus a monoclonal antibody against HER2 for metastatic breast cancer that overexpresses HER2. *N Engl J Med* 344:783–792.
18. Sepp-Lorenzino L, et al. (1996) Signal transduction pathways induced by heregulin in MDA-MB-453 breast cancer cells. *Oncogene* 12:1679–1687.
19. Hwang JY, et al. (2007) Multimode optical imaging of small animals: Development and applications. *Prog Biomed Opt Imaging* 8:1–10.
20. Karimi G, Ramezani M, Abdi A (2005) Protective effects of lycopene and tomato extract against doxorubicin-induced cardiotoxicity. *Phytother Res* 19:912–914.
21. Shuai Y, et al. (2007) Metallothionein protects against doxorubicin-induced cardiomyopathy through inhibition of superoxide generation and related nitrosative impairment. *Toxicol Lett* 170:66–74.
22. Gahery-Segard H, et al. (1998) Immune response to recombinant capsid proteins of adenovirus in humans: Antifiber and anti-penton base antibodies have a synergistic effect on neutralizing activity. *J Virol* 72:2388–2397.
23. Gahery-Segard H, et al. (1997) Humoral immune response to the capsid components of recombinant adenoviruses: Routes of immunization modulate virus-induced Ig subclass shifts. *Eur J Immunol* 27:653–659.
24. Yang Y, Greenough K, Wilson JM (1996) Transient immune blockade prevents formation of neutralizing antibody to recombinant adenovirus and allows repeated gene transfer to mouse liver. *Gene Ther* 3:412–420.
25. Dougherty TJ (1996) A brief history of clinical photodynamic therapy development at Roswell Park Cancer Institute. *J Clin Laser Med* 14:219–221.
26. Henderson BW, Sumlin AB, Owczarczak BL, Dougherty TJ (1991) Bacteriochlorophyll-a as photosensitizer for photodynamic treatment of transplantable murine tumors. *J Photochem Photobiol* 10:303–313.
27. Aviezer D, et al. (2000) Porphyrin analogues as novel antagonists of fibroblast growth factor and vascular endothelial growth factor receptor binding that inhibit endothelial cell proliferation, tumor progression, and metastasis. *Cancer Res* 60:2973–2980.
28. Hurley LH (2002) DNA and its associated processes as targets for cancer therapy. *Nat Rev* 2:188–200.
29. Billingham ME, Mason JW, Bristow MR, Daniels JR (1978) Anthracycline cardiomyopathy monitored by morphologic changes. *Cancer Treat Rep* 62:865–872.
30. Bristow MR, et al. (1978) Early anthracycline cardiotoxicity. *Am J Med* 65:823–832.
31. Sliwkowski MX, et al. (1994) Coexpression of erbB2 and erbB3 proteins reconstitutes a high affinity receptor for heregulin. *J Biol Chem* 269:14661–14665.
32. Goldman R, Levy RB, Peles E, Yarden Y (1990) Heterodimerization of the erbB-1 and erbB-2 receptors in human breast carcinoma cells: A mechanism for receptor transregulation. *Biochemistry* 29:11024–11028.
33. Jeschke M, et al. (1995) Targeted inhibition of tumor-cell growth by recombinant heregulin-toxin fusion proteins. *Int J Cancer* 60:730–739.
34. Hwang JY, et al. (2008) Large field of view scanning fluorescence lifetime imaging system for multi-mode optical imaging of small animals. *Prog Biomed Opt Imaging* 68590G:1–8.
35. Farkas DL (2003) Invention and commercialization in optical bioimaging. *Nat Biotechnol* 21:1269–1271.
36. Hara M, et al. (2003) Transgenic mice with green fluorescent protein-labeled pancreatic beta-cells. *Am J Physiol Endocrinol Metab* 284:E177–183.